ATLAS NOTE

ATLAS-CONF-2013-048

May 10, 2013

Search for direct top squark pair production in final states with two leptons in $\sqrt{s} = 8$ TeV pp collisions using 20 fb^{-1} of ATLAS data

The ATLAS Collaboration

Abstract

The results of a search for direct pair production of supersymmetric partners of the top quark are reported using 20.3 fb^{-1} of integrated luminosity from LHC pp collisions at 8 TeV collected by the ATLAS detector. Top squarks are searched for in events with two leptons (electrons or muons) in the final state. No excess above the Standard Model expectation is observed. Exclusion limits at 95% confidence level are placed on the mass of a top squark decaying as $\tilde{t}_1 \to \tilde{\chi}_1^{\pm} b \to \tilde{\chi}_1^0 W^{(*)} b$, for several assumptions on the hierarchy of the chargino $\tilde{\chi}_1^{\pm}$ and the lightest neutralino masses. Additionally, exclusion limits are placed for the first time on the mass of a top squark decaying directly via a three-body decay into $Wb\tilde{\chi}_1^0$.

ATLAS-CONF-2013-048
16 May 2013

1 Introduction

Partners of the top quark are an ingredient of several models addressing the hierarchy problem [1–4] of the Standard Model (SM). A boson partner would stabilize the Higgs boson mass against quadratically divergent quantum corrections, provided its mass is close to the electroweak symmetry breaking energy scale, making it accessible at the LHC [5]. One of these models is supersymmetry (SUSY) [6–14] which naturally resolves the hierarchy problem by introducing supersymmetric partners of the known bosons and fermions. In a generic R-parity conserving minimal supersymmetric extensions of the SM (MSSM) [15–19] the scalar partners of right-handed and left-handed quarks, $\tilde{q}_R$ and $\tilde{q}_L$, can mix to form two mass eigenstates. The lightest of the two top squark (stop) eigenstates is denoted $\tilde{t}_1$. Depending on the assumptions made on the SUSY model and the mass hierarchy of the sparticles, the stop might decay into a b-quark and a chargino, with a subsequent decay of the chargino into the lightest neutralino via a $W^{(*)}$ emission. If the chargino is heavier than the stop and $m(W) + m(b) < m(\tilde{t}_1) - m(\tilde{\chi}_1^0) < m(t)$, the dominant decay mode is expected to be the three-body $Wb\tilde{\chi}_1^0$ decay. In both scenarios, the final state from direct pair-production of top squarks has two $W^{(*)}$ bosons, two b-quarks, and two neutralinos. Depending on the decays of the two $W^{(*)}$ bosons zero, one or two isolated charged leptons are produced.

In this note, a search for top squarks in events characterized by the presence of two isolated leptons (e, μ) with opposite charge is reported. Significant missing transverse momentum, its magnitude referred to as $E_{\mathrm{T}}^{\mathrm{miss}}$, is expected from the neutralinos $\tilde{\chi}_1^0$ (assumed to be the lightest supersymmetric particle and stable) and neutrinos in the final state.

For these final state topologies, to separate the signal from the large SM background contributions dominated by top quark pair and W boson pair production, the m_{T2} variable [20, 21] was chosen as discriminating variable. It is defined as:

$$m_{\mathrm{T2}}(\mathbf{p}_{\mathrm{T}}^{\ell_1}, \mathbf{p}_{\mathrm{T}}^{\ell_2}, \mathbf{p}_{\mathrm{T}}^{\mathrm{miss}}) = \min_{\mathbf{q}_{\mathrm{T}}+\mathbf{r}_{\mathrm{T}}=\mathbf{p}_{\mathrm{T}}^{\mathrm{miss}}} \left\{ \max[\, m_{\mathrm{T}}(\mathbf{p}_{\mathrm{T}}^{\ell_1}, \mathbf{q}_{\mathrm{T}}), m_{\mathrm{T}}(\mathbf{p}_{\mathrm{T}}^{\ell_2}, \mathbf{r}_{\mathrm{T}}) \,] \right\},$$

where m_{T} indicates the transverse mass, $\mathbf{p}_{\mathrm{T}}^{\ell_1}$ and $\mathbf{p}_{\mathrm{T}}^{\ell_2}$ are the transverse momenta of the two leptons, and $\mathbf{q}_{\mathrm{T}}$ and $\mathbf{r}_{\mathrm{T}}$ are vectors which satisfy $\mathbf{q}_{\mathrm{T}} + \mathbf{r}_{\mathrm{T}} = \mathbf{p}_{\mathrm{T}}^{\mathrm{miss}}$. The minimization is performed over all the possible decompositions of $\mathbf{p}_{\mathrm{T}}^{\mathrm{miss}}$. The distribution of this variable for $t\bar{t}$ events presents a sharp kinematic end-point at the W boson mass [22, 23]. For stop pair production followed by $\tilde{t}_1 \to \tilde{\chi}^{\pm} b \to W^{(*)}\tilde{\chi}_1^0 b$ the kinematic limit is strongly correlated with the mass difference between the chargino and the neutralino, allowing for a good discrimination from the background for mass differences between the chargino and the neutralino larger than the W mass. For the direct three body decay, values of m_{T2} will have an end-point correlated with the difference between the mass of the stop and the mass of the neutralino, but the m_{T2} distribution will approach the kinematic limit with a much softer derivative than in the on-shell case.

The results are interpreted in various two-dimensional projections of a three-dimensional parameter space defined by the masses of the stop, the chargino and the neutralino for the two-body decay chain, while limits on the stop and neutralino masses are derived for the three-body decay.

A similar search for direct stop production has already been reported [24] based on the first 13 fb^{-1} of data collected by the ATLAS experiment in 2012. The present analysis is based on the full 2012 data, corresponding to an integrated luminosity of 20.3 fb^{-1}, and includes additional selections improving the parameter space coverage of the search in regions where there is a significant mass difference between stop and chargino. Previous ATLAS analyses using the 2011 data have placed exclusion limits on models with a top squark mass lighter than the top quark, for the stop decay mode into the lightest chargino and a b-jet [25, 26] and on models with an heavier stop quark decaying into a top quark and a neutralino [27–29]. Preliminary results on 2012 data placed further constraints on direct stop production assuming one of these decay modes [30–32]. The present analysis extends the sensitivity in the $m(\tilde{t}_1), m(\tilde{\chi}_1^{\pm}), m(\tilde{\chi}_1^0)$ parameter space and investigates for the first time the three-body decay mode.

2 The ATLAS detector

The ATLAS detector [33] consists of inner tracking devices surrounded by a superconducting solenoid, electromagnetic and hadronic calorimeters and a muon spectrometer with a toroidal magnetic field. The Inner Detector, in combination with the axial 2 T field from the solenoid, provides precision tracking of charged particles for $|\eta| < 2.5$[1]. It consists of a silicon pixel detector, a silicon strip detector and a straw tube tracker that also provides transition radiation measurements for electron identification. The calorimeter system covers the pseudorapidity range $|\eta| < 4.9$. It is composed of sampling calorimeters with either liquid argon or scintillating tiles as the active media. The muon spectrometer has separate trigger and high-precision tracking chambers which provide muon trigger and measurement capabilities for $|\eta| < 2.4$ and $|\eta| < 2.7$, respectively.

3 Monte Carlo samples

Monte Carlo (MC) simulated event samples are used to estimate the signal yields and to describe all the SM background processes leading to two prompt leptons. For the larger SM contributions, the shape of distributions of kinematic variables is taken from simulation, while the normalization is determined by measurements in appropriate control regions as described in Section 6. For the smaller backgrounds with two prompt leptons and for signal both the normalization and shapes are taken from simulation. Contributions from events where jets are misidentified as leptons or where leptons from a b-hadron or c-hadron decay are selected, collectively referred to as fake leptons in the following, are estimated from data as described in Section 6.

Top-quark pair production is simulated with POWHEG [34] interfaced to PYTHIA [35] for the fragmentation and the hadronization processes. The top-quark mass is fixed at 172.5 GeV, and the next-to-leading-order (NLO) parton distribution function (PDF) set CTEQ10 [36] is used. Additional samples are used to estimate the event generator systematic uncertainties: a POWHEG sample interfaced with HERWIG [37] and JIMMY [38]; a SHERPA [39] sample; two ACERMC [40] samples interfaced to PYTHIA for fragmentation and hadronization, where the parton shower parameters have been varied to produce additional radiation consistent with the experimental uncertainty in the data [41]. Samples of Wt events[2] are simulated with MC@NLO [42, 43], interfaced with HERWIG for the fragmentation and the hadronization processes, including JIMMY for the underlying event description. Samples of $t\bar{t}Z$ and $t\bar{t}W$ production are generated with MADGRAPH [44] interfaced to PYTHIA.

Samples of $Z/\gamma^{\star}$ produced in association with jets are generated with SHERPA using the PDF set CT10 [45] while ALPGEN samples are used in the estimate of systematic uncertainties. Diboson samples (WW, WZ, ZZ) are generated with POWHEG using the PDF set CT10. Additional samples generated with SHERPA are used for the evaluation of the event generator systematic uncertainties.

The background predictions are normalized to theoretical cross sections, calculated including higher-order QCD corrections where available, and are compared to data in appropriate control regions. The inclusive cross section for Z+jets is calculated with DYNNLO [46] with the MSTW 2008 NNLO PDF [47]. Approximate NLO+NNLL (next-to-next-to-leading-logarithm) cross sections are used in the normalization of the $t\bar{t}$ [48] and Wt [49] samples. Cross sections calculated at NLO are used for the diboson samples [42, 50] and for the $t\bar{t}W$ and $t\bar{t}Z$ [51] samples. Table 1 summarizes the production cross sections used in this analysis and their uncertainties.

[1] The pseudorapidity η is defined in terms of the angle θ with the beam pipe axis as $\eta = -\ln\tan(\theta/2)$

[2] s- and t-channel single top production samples have not been used since these processes do not produce two isolated leptons in the final state and their contribution is included in the data-driven estimate of events with fake leptons described in Section 6.

Table 1: The most important SM background processes and their production cross sections. For $t\bar{t}$ and $Z/\gamma^\star$, the production cross section is multiplied by the branching ratio of the leptonic decays indicated in the first column, where $\ell = e, \mu$, or τ. The last two columns give the perturbative order of the calculation and the reference for it.

Physics process	σ·BR [pb]	Perturbative order	Reference
$Z/\gamma^\star \to \ell\ell, m(\ell\ell) > 40$ GeV	1240 ± 60	DYNNLO	[46]
$t\bar{t} \to \ell + X$	129^{+12}_{-13}	NLO+NNLL	[48]
Wt	22.4 ± 1.5	NLO+NNLL	[49]
$t\bar{t}W$	0.231 ± 0.046	NLO	[51]
$t\bar{t}Z$	0.206 ± 0.021	NLO	[51]
WW	54.7 ± 3.3	NLO	[42, 50]
WZ	33.3 ± 1.7	NLO	[42, 50]
ZZ	11.2 ± 0.8	NLO	[42, 50]

Signal samples with a top squark that decays with unit probability into $\tilde{\chi}_1^\pm b$ are generated with MADGRAPH v5.1.4.8 interfaced to PYTHIA 6 [35] for the fragmentation and the hadronization processes. Signal samples with a top squark which decays exclusively into $\tilde{\chi}_1^0 Wb$ are generated with HERWIG++ [52].

Signal cross sections are calculated to NLO in perturbative QCD, including the resummation of soft gluon emission at next-to-leading-logarithmic accuracy (NLO+NLL) [53–55], as described in Ref. [56].

For all simulations, the generator parameters have been tuned to ATLAS data [57,58] and generated events have been processed through a detector simulation [59] based on GEANT4 [60], except for the $t\bar{t}$ POWHEG and signal samples which use fast detector simulation. Effects of multiple proton-proton interactions in the same bunch crossing (pile-up) are included, with the samples re-weighted so that the distribution of the average number of interactions per bunch crossing agrees with that in the data.

4 Physics object reconstruction

Proton-proton interaction vertex candidates are reconstructed using Inner Detector tracks. The vertex with the highest sum of the p_T^2 of the associated tracks is defined as the primary vertex.

Jets are reconstructed from three-dimensional calorimeter energy clusters using the anti-k_t jet algorithm [61, 62] with a radius parameter of 0.4. The measured jet energy is corrected with a local cluster calibration [63] to account for various effects of non-compensation, dead material and out-of-cluster energy deposits. Final jet energy scale corrections, and corrections for in-time and out-of-time pile-up are also applied, as described in Ref. [64]. Only jet candidates with $p_{\mathrm{T}} > 20$ GeV, $|\eta| < 2.5$ are retained. Jet candidates with 20 GeV $< p_{\mathrm{T}} <$ 50 GeV and $|\eta| < 2.4$ are also required to have a "jet vertex fraction" larger than 0.5. Based on tracking information this variable quantifies the fraction of the total momentum of tracks associated to the jet that originates from the reconstructed primary vertex. This requirement rejects jets originating from additional proton-proton interactions occurring in the same bunch crossing. Events with jets failing the jet quality criteria designed to reject noise and non-collision backgrounds [64] are vetoed.

Electron candidates are required to have $p_{\mathrm{T}} > 10$ GeV, $|\eta| < 2.47$ and to satisfy "medium" electromagnetic shower shape and track selection quality criteria [65]. These preselected electrons are then required to pass "tight" quality criteria [65] which place additional requirements on the ratio of calorimetric energy to track momentum, and on the fraction of hits in the straw tube tracker required to pass a higher threshold for transition radiation. The electron candidates are then required to be isolated: the

scalar sum, Σp_{T}, of the p_{T} of Inner Detector tracks with $p_{\mathrm{T}} > 1$ GeV, not including the electron track, within a cone in the $\eta - \phi$ plane of radius $\Delta R = \sqrt{\Delta\eta^2 + \Delta\phi^2} = 0.2$ around the electron candidate, must be less than 10% of the electron p_{T}.

Muon candidates are reconstructed using either a full muon spectrometer track matched to an Inner Detector track, or a muon spectrometer segment matched to an extrapolated Inner Detector track [66]. They must be reconstructed with sufficient hits in the pixel, strip and straw tube detectors. They are required to have $p_{\mathrm{T}} > 10$ GeV, $|\eta| < 2.4$ and must have longitudinal and transverse impact parameters within 1 mm and 0.2 mm of the primary vertex, respectively. Such preselected candidates are then required to have $\Sigma p_{\mathrm{T}} < 1.8$ GeV, defined in analogy to the electron case.

Following the object reconstruction described above, overlaps between jet, electron and muon candidates are resolved as follows: any jet within $\Delta R = 0.2$ of preselected electrons is discarded; electrons or muons within $\Delta R = 0.4$ of any remaining jet are discarded to reject leptons from the decay of a b- or c-hadron.

The measurement of $E_{\mathrm{T}}^{\mathrm{miss}}$ is based on the transverse momenta of all jets and lepton candidates and all calorimeter clusters not associated to these objects [67]. The unassociated clusters are calibrated at the electromagnetic scale.

5 Event selection

This search uses proton-proton collisions recorded at a centre-of-mass energy of 8 TeV. Data were collected based on the decision of a three-level trigger system. Events are accepted if they passed either a single-electron, a single-muon, a double-electron, a double-muon, or an electron-muon trigger. The trigger efficiency exceeds 99% for the events passing the full selection described below. After beam, detector and data quality requirements, a total integrated luminosity of 20.3 fb^{-1} is used.

Events are required to have exactly two opposite-sign (OS) leptons (electrons or muons). At least one electron or muon must have a momentum larger than 25 GeV, in order to be in the trigger efficiency plateau regions described above, and the invariant mass of the two leptons is required to be larger than 20 GeV. If the event contains a third preselected electron or muon, the event is rejected. In order to reduce the number of background events containing two leptons produced by the on-shell decay of the Z boson, the invariant mass of the same-flavour lepton pairs is required to be outside the $71 - 111$ GeV range.

Two additional selections are applied to reduce the number of background events with high m_{T2} arising from events with large $E_{\mathrm{T}}^{\mathrm{miss}}$ due to mismeasured jets: $\Delta\phi_b < 1.5$ and $\Delta\phi > 1$. The quantity $\Delta\phi_b$ is the azimuthal angle between the $\mathbf{p}_{\mathrm{T}}^{\mathrm{miss}}$ vector and the $\mathbf{p}_{\mathrm{Tb}}^{\ell\ell} = \mathbf{p}_{\mathrm{T}}^{\mathrm{miss}} + \mathbf{p}_{\mathrm{T}}^{\ell_1} + \mathbf{p}_{\mathrm{T}}^{\ell_2}$ vector, introduced in Ref. [68]. The $\mathbf{p}_{\mathrm{Tb}}^{\ell\ell}$ variable, with magnitude $p_{\mathrm{Tb}}^{\ell\ell}$, is the opposite of the vector sum of all the transverse hadronic activity in the event. For WW and $t\bar{t}$ backgrounds it measures the transverse boost of the WW system, and for the signal the transverse boost of the chargino-chargino system. The $\Delta\phi$ variable is the azimuthal angle difference between the $\mathbf{p}_{\mathrm{T}}^{\mathrm{miss}}$ vector and the direction of the closest jet.

After these selections the background is dominated by $t\bar{t}$ events for different-flavour (DF) lepton pairs, and $Z/\gamma^\star$+jets for same-flavour (SF) lepton pairs. The m_{T2} distribution for $Z/\gamma^\star$+jets background is, however, steeply falling and by requiring $m_{\mathrm{T2}} > 40$ GeV, the $t\bar{t}$ becomes the dominant background in the SF sample as well.

Four signal regions (SRs) are then defined, with different selections on m_{T2} and on the transverse momenta of the two leading jets, as reported in Table 2. SR M90 has the loosest selection, requiring $m_{\mathrm{T2}} > 90$ GeV and no additional requirements on jets. It provides sensitivity to scenarios with a small difference between the masses of the top squark and the chargino, so that the production of high p_{T} jets is not expected. SR M110 and M120 have a loose selection on jets, requiring two jets with $p_{\mathrm{T}} > 20$ GeV, and they require m_{T2} to be larger than 110 GeV and 120 GeV, respectively. They provide sensitivity to

scenarios with small to moderate values of $m(\tilde{t}_1) - m(\tilde{\chi}_1^{\pm})$ resulting in moderate jet activity [3]. SR M100 has tighter jet selections, and provides sensitivity to scenarios with both large $m(\tilde{t}_1) - m(\tilde{\chi}_1^{\pm})$ and large $m(\tilde{\chi}_1^{\pm}) - m(\tilde{\chi}_1^{0})$.

SR	M90	M100	M110	M120
p_{T} leading lepton	> 25 GeV			
$\Delta\phi(E_{\mathrm{T}}^{\mathrm{miss}}$, closest jet)	> 1.0			
$\Delta\phi(E_{\mathrm{T}}^{\mathrm{miss}}, p_{\mathrm{Tb}}^{\ell\ell})$	< 1.5			
m_{T2}	> 90 GeV	> 100 GeV	> 110 GeV	> 120 GeV
p_{T} leading jet	no selection	> 100 GeV	> 20 GeV	> 20 GeV
p_{T} second jet	no selection	> 50 GeV	> 20 GeV	> 20 GeV

Table 2: Signal regions used in the analysis.

6 Background estimation

The dominant SM background contributions to the SR are top and W pair production. Other diboson processes are also expected to contribute significantly: WZ in its 3-lepton decay mode, and ZZ decaying to two leptons and two neutrinos. These backgrounds are evaluated defining three control regions (CR) and using MC simulation to extrapolate the rate measured in the CRs to the expected background yield in the SRs. The three control regions are defined as:

- **CRT**, defined by DF events with 40 GeV $< m_{\mathrm{T2}} <$ 80 GeV, and $p_{\mathrm{Tb}}^{\ell\ell} > 30$ GeV, and passing all the SR selections on other variables. These regions are populated mostly by $t\bar{t}$ events.
- **CRW**, defined by DF events with 40 GeV $< m_{\mathrm{T2}} <$ 80 GeV, $p_{\mathrm{Tb}}^{\ell\ell} <$ 15 GeV, $\Delta\phi > 1.0$ and $\Delta\phi_b < 1.5$. The same control region is used for all SRs. This region is populated mostly by WW events.
- **CRZ**, defined by SF events with an invariant mass in the 71 − 111 GeV range, $m_{\mathrm{T2}} > 90$ GeV, $\Delta\phi > 1.0$ and $\Delta\phi_b < 1.5$. This region is populated mostly by WZ and ZZ events.

For each SR there is a corresponding CRT, except for SR M110 and M120 for which the control region is the same. CRW and CRZ are instead in common for all SRs[4].
With this approach, the ratio of events for each of the background sources in the CRs and SRs is taken from MC, and the normalisation from data. Systematic uncertainties in the MC simulation affect the ratio of the expected yields in the different regions and are taken into account to determine the uncertainty on the background prediction. For each SR, the evaluation is performed by means of a likelihood fit with the observed events in the three CRs as constraints, and the normalisation terms for each of the three backgrounds ($t\bar{t}$, WW, and the sum of WZ and ZZ) as free parameters.The systematic uncertainties are described by nuisance parameters, but are not constrained by the fit. Each uncertainty source is described by a single nuisance parameter, and all correlations between background processes and selections are taken into account. The list of systematic uncertainties considered is described in the next section.

[3] An explicit requirement that b-tagged jets were present was considered but found not to increase the sensitivity. While it reduces the diboson background component, it is less effective to reject background from top pair production and reduces the signal acceptance.

[4] The possibility to use a dedicated CRW and CRZ for each SR was considered but found to be impractical, because adding jet selections to CRW lowers the purity of the targeted background process while adding the jet selection to CRZ results in an increased statistical uncertainty.

Table 3: Results of the background determination from fits for the various control regions using the selection cuts for the M90 signal region. CRTM90, CRW and CRZ are the $t\bar{t}$, WW, and $WZ + ZZ$ control regions, respectively. The estimated numbers for the validation regions VRSF and VRDF, defined as those events with 80 GeV $< m_{\mathrm{T2}} <$ 90 GeV and passing all other signal region selections (see text), are also given. The total expected background is computed using the normalizations from the fit and it is constrained to be equal to the observed number of events in the control regions. Nominal background expectations (normalized to the theoretical cross section) are given for comparison for these backgrounds (top and vector boson pair production) which are normalized to data. Combined statistical, experimental and theoretical systematic uncertainties are indicated. Events with fake leptons are estimated with the data-driven technique described in Section 6. A horizontal dash indicates a negligible contribution.

Process	CRTM90	CRW	CRZ	VRSF	VRDF
Observed events	11615	854	169	478	603
Expected bkg events	11615 ± 110	854 ± 27	169 ± 13	450 ± 50	600 ± 40
Fitted $t\bar{t}$ events	8300 ± 400	142 ± 26	27 ± 6	300 ± 40	410 ± 30
Fitted WW events	1500 ± 290	580 ± 40	9.7 ± 2.0	87 ± 17	108 ± 21
Fitted WZ, ZZ events	60 ± 9	13 ± 4	112 ± 15	5.7 ± 1.4	2.3 ± 1.7
Expected Z+jets events	26 ± 27	0.7 ± 0.8	17 ± 7	4 ± 6	-
Expected $t\bar{t}V$ events	10 ± 3	-	0.6 ± 0.2	0.5 ± 0.2	0.8 ± 0.3
Expected Wt events	1050 ± 80	34 ± 7	1.6 ± 1.1	39 ± 7	54 ± 9
Events with fake leptons	710 ± 220	82 ± 17	-	11 ± 7	18 ± 8
Fit input, expectation $t\bar{t}$	8100 ± 1000	138 ± 25	27 ± 9	290 ± 50	400 ± 60
Fit input, expectation WW	1160 ± 120	450 ± 60	7.5 ± 1.1	67 ± 7	83 ± 8
Fit input, expectation WZ, ZZ	67 ± 9	15 ± 7	125 ± 26	6.3 ± 2.5	2.6 ± 1.4

Table 4: Results of the background determination from fits for the various control regions using the selection cuts for the M100 signal region. CRTM100, CRW and CRZ are the $t\bar{t}$, WW, and $WZ + ZZ$ control regions, respectively. The estimated numbers for the validation regions VRSF and VRDF, defined as those events with 80 GeV $< m_{\mathrm{T2}} <$ 90 GeV and passing all other signal region selections (see text), are also given. The total expected background is computed using the normalizations from the fit and it is constrained to be equal to the observed number of events in the control regions. Nominal background expectations (normalized to the theoretical cross section) are given for comparison for these backgrounds (top and vector boson pair production) which are normalized to data. Combined statistical, experimental and theoretical systematic uncertainties are indicated. Events with fake leptons are estimated with the data-driven technique described in Section 6. A horizontal dash indicates a negligible contribution.

Process	CRTM100	CRW	CRZ	VRSF	VRDF
Observed events	1322	854	169	60	66
Total expected bkg events	1322 ± 38	854 ± 27	169 ± 12	48 ± 10	62 ± 9
Fitted $t\bar{t}$ events	1180 ± 40	150 ± 40	29 ± 8	41 ± 10	57 ± 8
Fitted WW events	37 ± 11	580 ± 50	10 ± 2	1.3 ± 0.6	1.6 ± 0.9
Fitted WZ, ZZ events	1.3 ± 0.7	13 ± 4	112 ± 19	0.1 ± 0.1	0.1 ± 0.2
Expected Z+jets events	0.9 ± 1.1	0.7 ± 0.8	17 ± 7	0.3 ± 0.5	-
Expected $t\bar{t}V$ events	3.9 ± 1.2	-	0.6 ± 0.2	0.16 ± 0.08	0.3 ± 0.1
Expected Wt events	60 ± 10	34 ± 7	1.6 ± 1.1	2.1 ± 1.5	1.4 ± 2.4
Expected events with fake leptons	42 ± 19	82 ± 18	-	3.0 ± 2.1	1.3 ± 0.8
Fit input, expectation $t\bar{t}$	1090 ± 190	138 ± 25	27 ± 9	38 ± 12	53 ± 14
Fit input, expectation WW	29 ± 9	450 ± 60	7.7 ± 1.1	1.0 ± 0.8	1.3 ± 1.1
Fit input, expectation WZ, ZZ	1.5 ± 1.6	15 ± 7	125 ± 26	0.1 ± 0.1	0.1 ± 0.2

Table 5: Results of the background determination from fits for the various control regions using the selection cuts for the M110 and M120 signal regions. CRTM110, CRW and CRZ are the $t\bar{t}$, WW, and WZ+ZZ control regions, respectively. The estimated numbers for the validation regions VRSF and VRDF, defined as those events with 80 GeV $< m_{\mathrm{T2}} <$ 90 GeV and passing all other signal region selections (see text), are also given. The total expected background is computed using the normalizations from the fit and it is constrained to be equal to the observed number of events in the control regions. Nominal background expectations (normalized to the theoretical cross section) are given for comparison for these backgrounds (top and vector boson pair production) which are normalized to data. Combined statistical, experimental and theoretical systematic uncertainties are indicated. Events with fake leptons are estimated with the data-driven technique described in Section 6. A horizontal dash indicates a negligible contribution.

Process	CRTM110	CRW	CRZ	VRSF	VRDF
Observed events	7872	854	169	306	370
Expected total bkg events	7872 ± 90	854 ± 29	169 ± 12	270 ± 30	370 ± 30
Fitted $t\bar{t}$ events	6910 ± 120	153 ± 15	30 ± 7	240 ± 30	330 ± 30
Fitted WW events	270 ± 30	570 ± 30	10.2 ± 2.1	11 ± 2	13 ± 3
Fitted WZ, ZZ events	12 ± 2	13 ± 3	110 ± 15	1.1 ± 0.4	0.2 ± 0.2
Expected Z+jets events	3.5 ± 1.1	0.7 ± 0.8	17 ± 7	1.2 ± 1.1	-
Expected $t\bar{t}V$ events	9.7 ± 2.3	-	0.6 ± 0.2	0.42 ± 0.16	0.7 ± 0.2
Expected Wt events	420 ± 30	34 ± 7	1.6 ± 1.1	12 ± 4	18 ± 4
Events with fake leptons	250 ± 100	82 ± 18	-	5 ± 4	9 ± 4
Fit input, expectation $t\bar{t}$	6200 ± 700	138 ± 25	27 ± 9	210 ± 40	290 ± 50
Fit input, expectation WW	220 ± 30	450 ± 60	7.5 ± 1.1	8.8 ± 1.2	10 ± 3
Fit input, expectation WZ, ZZ	14 ± 4	15 ± 7	125 ± 26	1.2 ± 0.4	0.3 ± 0.3

Additional SM processes yielding two isolated leptons and $E_{\mathrm{T}}^{\mathrm{miss}}$ (Wt, Z+jets, $t\bar{t}W$ and $t\bar{t}Z$), and providing a sub-dominant contribution to the SRs are determined from MC simulation.

The fake lepton background consists of semi-leptonic $t\bar{t}$, s-channel and t-channel single top, W+jets and light- and heavy-flavour multijet events. The contribution from this background is small (less than 10% of the total background). It is estimated from data with a method similar to that described in Refs. [69, 70]. Two types of lepton identification criteria are defined for this evaluation: "tight", corresponding to the full set of identification criteria described above, and "loose", corresponding to preselected electrons and muons. The method counts the number of observed events containing loose-loose, loose-tight, tight-loose and tight-tight lepton pairs in a given SR (loose-tight refers to events with the highest p_{T} lepton being loose and the lower p_{T} one being tight, and tight-loose to the opposite).The probability for real leptons passing the loose selection criteria to also pass the tight selection is measured using a $Z \to \ell\ell$ ($\ell = e, \mu$) sample. The equivalent probability for fake leptons is measured from multijet-enriched control samples. The number of events containing a contribution from one or two fake leptons is calculated from these probabilities.

The result of the background fit as well as the expected background composition before the fit are reported in Tables 3-5. To verify the extrapolation procedure, the predicted background is compared to the observed rate for events in validation regions VRSF and VRDF, defined as the SF and DF events respectively, which pass all the signal region cuts but with 80 GeV $< m_{\mathrm{T2}} <$ 90 GeV. The results are reported in the last two columns of Tables 3-5. In all the six validation regions, the observed numbers of events are in agreement with the predicted event yields, the largest discrepancy being 1.1 standard deviations.

Figure 1 shows the $p_{\mathrm{Tb}}^{\ell\ell}$ distribution for DF events with 40 GeV $< m_{\mathrm{T2}} <$ 80 GeV, $\Delta\phi > 1.0$ and $\Delta\phi_b < 1.5$. The range $p_{\mathrm{Tb}}^{\ell\ell} <$ 15 GeV corresponds to the WW CR while the events with $p_{\mathrm{Tb}}^{\ell\ell} >$ 30 GeV are those entering in CRTM90. Here the background predictions are estimated from the MC simulation before applying the normalizations from the background fit, with the exception of the events with fake leptons which are estimated from data as described above. The figure shows a reasonable agreement between the data and the predictions from the MC simulation for this distribution; the excess of about 20% observed in the data for low values of $p_{\mathrm{Tb}}^{\ell\ell}$ is compensated by the background fit by increasing the WW normalization, as can be seen by comparing the fit input and fitted WW yields in Table 3.

Figure 2 shows the m_{T2} distribution for SF events with $p_{\mathrm{Tb}}^{\ell\ell} <$ 15 GeV, $\Delta\phi > 1.0$ and $\Delta\phi_b < 1.5$ and invariant mass within 20 GeV of the Z boson mass. The events with $m_{\mathrm{T2}} >$ 90 GeV in the figure are those entering CRZ. The data are in good agreement with the background expectations for all values of m_{T2}.

7 Systematic Uncertainties

Various systematic uncertainties affecting the predicted background rates in the signal regions are considered. Such uncertainties are either used directly in the evaluation of the predicted background in the SR when the background is derived by MC, or to compute the uncertainty on the ratio of the expected events in the CRs and SRs and propagate it to the predicted event yields in the SR when the background normalization is constrained from the CR. The following experimental systematic uncertainties are found to be non-negligible:

Jet energy scale and resolution: the uncertainty on the jet energy scale (JES) has been derived using a combination of MC simulation and data [64] and varies as a function of the jet p_{T} and pseudorapidity. Additional systematic uncertainties arise from the dependence of the jet response on the number of interactions per bunch crossing and on the jet flavour. The components of the jet energy scale uncertainty are varied by $\pm 1\sigma$ in the MC simulation and propagated to the expected event yield. Uncertainties related to the jet energy resolution (JER) are obtained with an in situ measurement of the jet response asymmetry

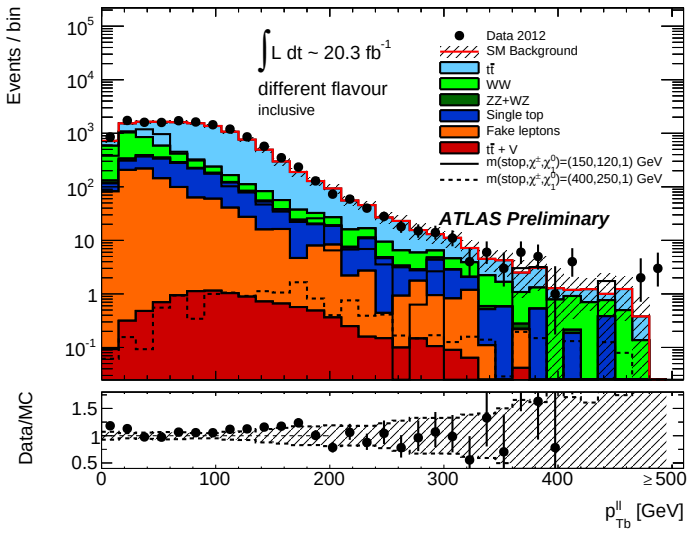

Figure 1: Distribution of $p_{\mathrm{Tb}}^{\ell\ell}$ for DF events with 40 GeV $< m_{\mathrm{T2}} <$ 80 GeV, $\Delta\phi > 1.0$ and $\Delta\phi_b < 1.5$. The contributions from all SM backgrounds are shown; the bands represent the total uncertainty. The components labelled "fake lepton" are estimated from data as described in the text; the other backgrounds are estimated from MC simulation.The expected distribution for two signal models is also shown: the full line corresponds to a model with m($\tilde{t}_1$)=150 GeV, m($\tilde{\chi}_1^{\pm}$)=120 GeVand m($\tilde{\chi}_1^0$)=1 GeV; the dashed line to a model with m($\tilde{t}_1$) = 400 GeV, m($\tilde{\chi}_1^{\pm}$) = 250 GeV and m($\tilde{\chi}_1^0$)=1 GeV.

in dijet events [71]. Their impact on the event yields is estimated by applying an additional smearing to the jet transverse momenta in the MC simulation. The JES and JER variations applied to jets are propagated to the $E_{\mathrm{T}}^{\mathrm{miss}}$.

Calorimeter cluster energy scale, resolution and pile-up modelling: the uncertainties related to the contribution to $E_{\mathrm{T}}^{\mathrm{miss}}$ from the energy scale and resolution of the calorimeter cells not associated to electrons, muons or jets, and also from low momentum (7 GeV $< p_{\mathrm{T}} <$ 25 GeV) jets, as well as the uncertainty due to the modelling of pile-up have been evaluated as described in Ref. [67].

Fake-lepton background uncertainties: an uncertainty on the fake background is assigned from the statistics of the control samples used to measure the probabilities to pass the tight selection, from the comparison of results obtained with these probabilities computed with alternative control samples, and from the number of events of the loose and tight event samples.

The uncertainties in the lepton reconstruction efficiency and in the trigger modelling have a negligible impact on the analysis. A ±2.8% uncertainty on the luminosity determination was measured using techniques similar to that described in Ref. [72] from a preliminary calibration of the luminosity scale derived from beam-separation scans performed in November 2012. It is included for all signal and background MC simulations.

The leading theoretical uncertainties are due to the modelling of the diboson background, evaluated comparing the predictions of Sherpa and Powheg, and of the top pair background, evaluated comparing the predictions of Powheg and Sherpa for the matrix element calculation, the predictions of Pythia and Herwig for the parton showering and hadronization, and the predictions of two AcerMC samples with different tunings for the uncertainties related to the amount of initial and final state radiation.

Other significant sources of uncertainty are the limited number of events in the CRs and MC simula-

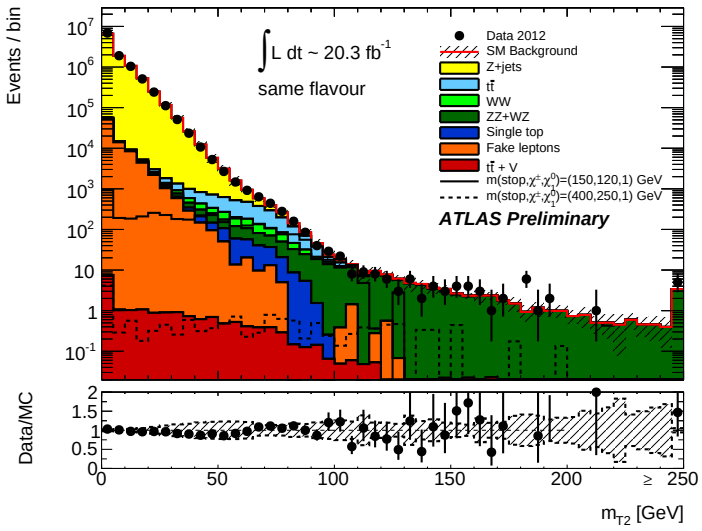

Figure 2: Distribution of m_{T2} for SF events with a di-lepton invariant mass in the 71-111 GeV range, $\Delta\phi > 1.0$ and $\Delta\phi_b < 1.5$. The contributions from all SM backgrounds are shown; the bands represent the total uncertainty. The components labelled "fake lepton" are estimated from data as described in the text; the other backgrounds are estimated from MC simulation.The expected distribution for two signal models is also shown: the full line corresponds to a model with m($\tilde{t}_1$)=150 GeV, m($\tilde{\chi}_1^{\pm}$)=120 GeVand m($\tilde{\chi}_1^0$)=1 GeV; the dashed line to a model with m($\tilde{t}_1$) = 400 GeV, m($\tilde{\chi}_1^{\pm}$) = 250 GeV and m($\tilde{\chi}_1^0$)=1 GeV.

tion samples.

A summary of the uncertainties on the total expected background is given in Table 6. The row labelled "samples size" includes the effects of the limited number of data events in the CRs and the limited number of MC simulated events.

Table 6: Systematic uncertainties for the four signal regions: the variations in the predicted background yield are quoted. It should be noted that the individual uncertainties can be correlated.

	M90	M100	M110	M120
jet energy scale and resolution	6%	22%	7%	5%
cluster energy scale and resolution	5%	24%	5%	5%
pile-up	6%	6%	3%	7%
diboson generator	3%	4%	8%	14%
top generator	3%	6%	11%	5%
top ISR/FSR	2%	6%	1%	5%
top parton shower	4%	19%	27%	7%
samples size	3%	17%	11%	19%
$t\bar{t}$ normalization	3%	4%	1%	0%
WW normalization	4%	2%	2%	2%
WZ/ZZ normalization	1%	0%	1%	2%
Fake-lepton uncertainties	2%	0%	1%	2%
Total uncertainty	12%	46%	35%	28%

Experimental systematic uncertainties are also evaluated for the expected signal yields.

The uncertainty on the signal cross section predictions is calculated with an envelope of cross section values which is defined using the 68% confidence level (CL) ranges of the CTEQ [73] (including the α_s uncertainty) and MSTW [47] PDF sets, together with variations of the factorization and renormalization scales by factors of two or one half. The nominal cross section value is taken to be the midpoint of the envelope and the uncertainty assigned is half the full width of the envelope, using the procedure described in Ref. [56]. The typical cross section uncertainty is ±15% for the top squark signal.

8 Results

Figure 3 shows the distributions of the m_{T2} variable after applying all the selection criteria of SR M90 except that on m_{T2}. The components labelled "fake lepton" are estimated from data as described in Section 6; the other backgrounds are estimated from MC simulation with normalizations measured in CRs described in Section 6 for $t\bar{t}$ and diboson backgrounds. For illustration, the distributions for two signal models are also shown. The equivalent distributions for SR M100 and M110/120 are shown in Figs. 4 and 5, respectively. The data agree with the SM background expectation within uncertainties.

Table 7 shows the expected numbers of events in the four SRs for each background source and the observed numbers of events. The sum of events in the same and opposite flavour channel is reported. No excess of events is observed in data. Limits at 95% CL are derived on the visible new physics cross section $\sigma_{\mathrm{vis}} = \sigma \times \epsilon \times \mathcal{A}$, where σ is the total production cross section for a non-SM signal, $\mathcal{A}$ is the acceptance defined by the fraction of events passing the geometric and kinematic selections at particle level, and ϵ is the detector reconstruction, identification and trigger efficiency. This limit assumes that the new physics does not contaminate the CRs. Limits are set using the confidence level (CL_s) likelihood ratio prescription as described in Ref. [74]. Systematic uncertainties are included in the likelihood function as nuisance parameters with a Gaussian probability density function. All uncertainties previously described are taken into account, as well as those due to the detector response and the integrated luminosity. The detector response uncertainty on the signal yield are typically between ±5% and ±20%, while the theoretical uncertainty is about ±15%. For low stop mass, the MC statistics becomes the dominant uncertainty in the tighter SR (M100, M110, M120). For each signal hypothesis, the fit of the top pair and boson pair normalization is re-done taking into account the signal contamination in the control regions.

The results obtained are used to derive limits on the mass of a pair-produced scalar top $\tilde{t}_1$ decaying with 100% branching ratio into the lightest chargino and a b-quark. For each point the SR giving the best expected sensitivity is used to set the limits. The sensitivity of this search depends on three parameters, namely the scalar top, lightest chargino and neutralino masses. Two-dimentional slices are made to quantify the exclusion limits on these parameters: in the stop–chargino mass plane for a neutralino with a mass of 1 GeV (Fig. 6); in the stop–neutralino mass plane for a fixed value of $m(\tilde{t}) - m(\tilde{\chi}_1^{\pm}) = 10$ GeV (Fig. 7); in the chargino–neutralino mass plane for a fixed 300 GeV stop quark mass (Fig. 8); in the stop–neutralino mass plane for $m(\tilde{\chi}_1^{\pm}) = 2m(\tilde{\chi}_1^0)$ (Fig. 9); and in the stop–neutralino mass plane for a fixed 150 GeV chargino mass (Fig. 10).

A scalar top quark of mass between 150 and 442 GeV is excluded at 95% CL for a neutralino with a mass of 1 GeV and approximately degenerate chargino and scalar top quark masses. For a neutralino and a chargino with masses of 1 GeV and 200 GeV, respectively, the 95% CL exclusion range on the scalar top quark mass is 200 − 420 GeV.

In Figure 11 the limits on the mass of a top squark decaying with 100% branching ratio to $bW\tilde{\chi}_1^0$ are reported in the plane defined by the scalar top and neutralino masses. For a value of $m(\tilde{t}_1) - m(\tilde{\chi}_1^0)$ equal to 90 GeV, 130 GeV, and 160 GeV top squark masses lower than 155 GeV, 220 GeV, and 200 GeV, respectively, are excluded. The sensitivity of the analysis is best for intermediate values of $m(\tilde{t}_1) - m(\tilde{\chi}_1^0)$ and decreases approaching either the lower ($m(\tilde{t}_1) - m(\tilde{\chi}_1^0) = m(W) + m(b)$) or upper ($m(\tilde{t}_1) - m(\tilde{\chi}_1^0) = m(t)$)

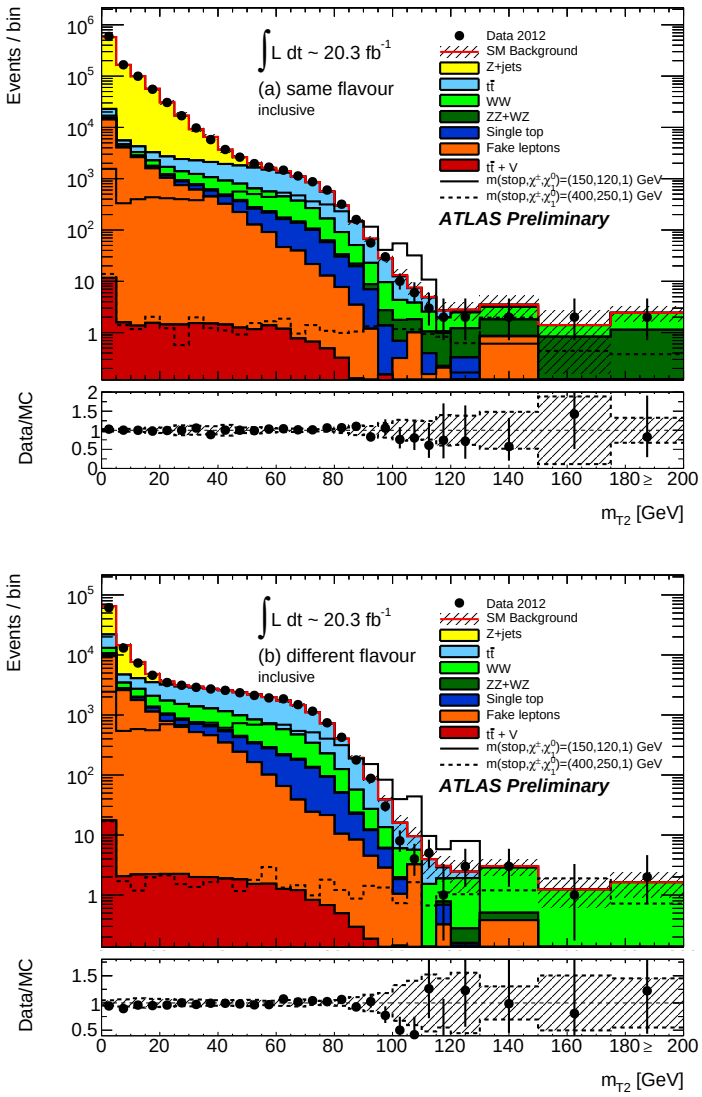

Figure 3: Distributions of m_{T2} for events passing all the signal candidate selection requirements, except that on m_{T2}, of the M90 selection, for (a) SF and (b) DF events. The contributions from all SM backgrounds are shown; the bands represent the total uncertainty. The components labelled "fake lepton" are estimated from data as described in the text; the other backgrounds are estimated from MC simulation with normalizations measured in control regions described in Section 6 for $t\bar{t}$ and diboson backgrounds.The expected distributions for two signal models are also shown: the full line corresponds to a model with m($\tilde{t}_1$)=150 GeV, m($\tilde{\chi}_1^{\pm}$)=120 GeV and m($\tilde{\chi}_1^0$)=1 GeV; the dashed line to a model with m($\tilde{t}_1$) = 400 GeV, m($\tilde{\chi}_1^{\pm}$) = 250 GeV and m($\tilde{\chi}_1^0$)=1 GeV.

kinematic limits. In both cases this is due to a decrease of the acceptance of the m_{T2} cut. For low values of $m(\tilde{t}_1) - m(\tilde{\chi}_1^0)$ this is due to the decrease of the kinematic endpoint for this variable at truth level. For high values of $m(\tilde{t}_1) - m(\tilde{\chi}_1^0)$ the endpoint increases but kinematic configurations with m_{T2} close to the endpoint are strongly disfavored by the top quark propagator, which enhances kinematic configurations with high Wb invariant mass and low $\tilde{\chi}_1^0$ momenta.

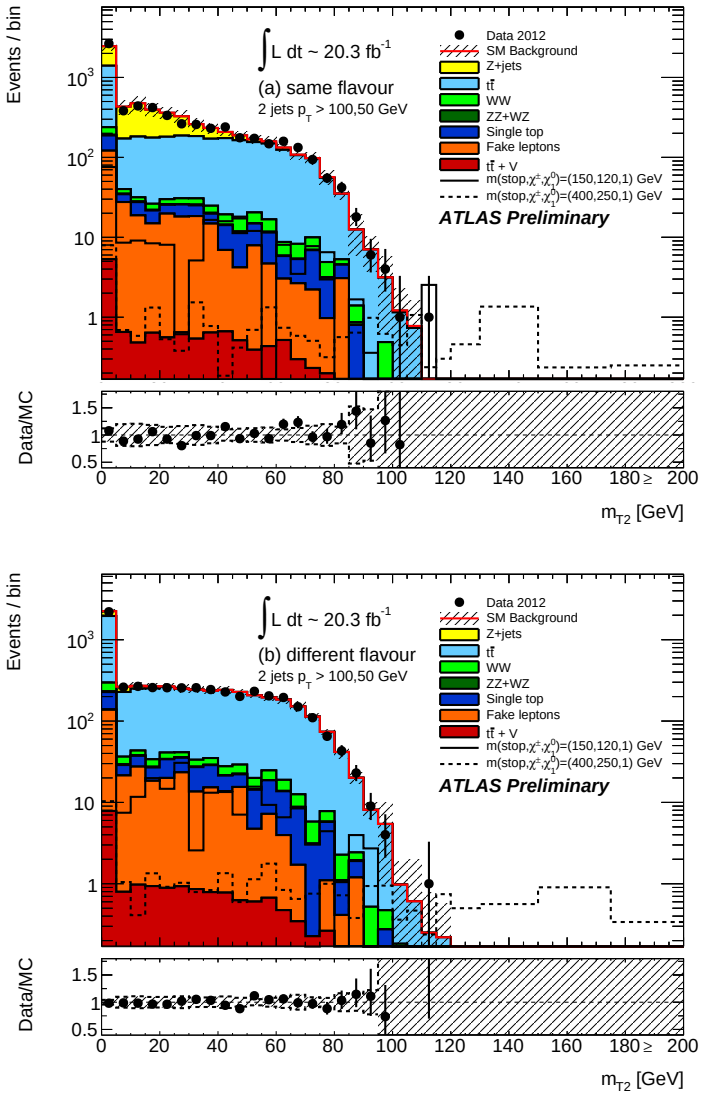

Figure 4: Distributions of m_{T2} for events passing all the signal candidate selection requirements, except that on m_{T2}, of the M100 selection, for (a) SF and (b) DF events. The contributions from all SM backgrounds are shown; the bands represent the total uncertainty. The components labelled "fake lepton" are estimated from data as described in the text; the other backgrounds are estimated from MC simulation with normalizations measured in control regions described in Section 6 for $t\bar{t}$ and diboson backgrounds.The expected distributions for two signal models are also shown: the full line corresponds to a model with m($\tilde{t}_1$)=150 GeV, m($\tilde{\chi}_1^{\pm}$)=120 GeV and m($\tilde{\chi}_1^0$)=1 GeV; the dashed line to a model with m($\tilde{t}_1$) = 400 GeV, m($\tilde{\chi}_1^{\pm}$) = 250 GeV and m($\tilde{\chi}_1^0$)=1 GeV.

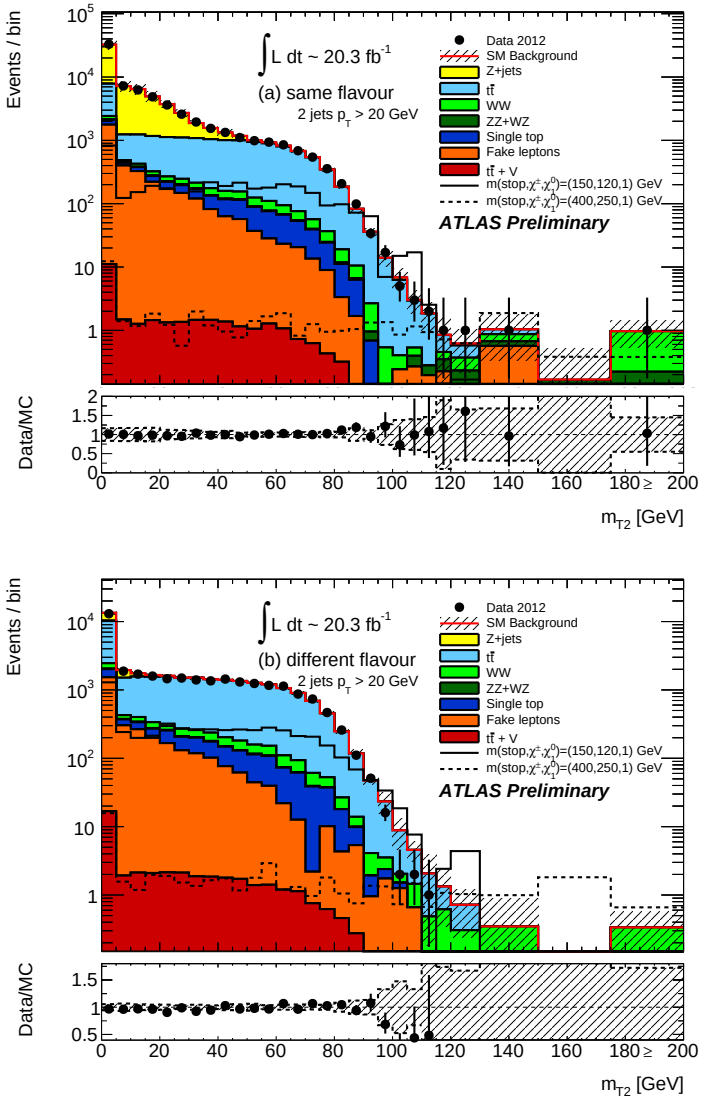

Figure 5: Distributions of m_{T2} for events passing all the signal candidate selection requirements, except that on m_{T2}, of the M110 and M120 selections, for (a) SF and (b) DF events. The contributions from all SM backgrounds are shown; the bands represent the total uncertainty. The components labelled "fake lepton" are estimated from data as described in the text; the other backgrounds are estimated from MC simulation with normalizations measured in control regions described in Section 6 for $t\bar{t}$ and diboson backgrounds.The expected distributions for two signal models are also shown: the full line corresponds to a model with m($\tilde{t}_1$)=150 GeV, m($\tilde{\chi}_1^{\pm}$) = 120 GeV and m($\tilde{\chi}_1^0$)=1 GeV; the dashed line to a model with m($\tilde{t}_1$) = 400 GeV, m($\tilde{\chi}_1^{\pm}$) = 250 GeV and m($\tilde{\chi}_1^0$)=1 GeV.

Table 7: Numbers of events observed in 20.3 fb^{-1} of data at 8 TeV centre-of-mass energy, in the M90, M100, M110, and M120 signal regions, compared with background expectations obtained from the fits described in the text. The expectations (normalised to theoretical cross-sections) are given for comparison for those backgrounds (top and boson pair production) which are normalized to data. Combined statistical, experimental and theoretical systematic uncertainties are indicated.

Process	M90	M100	M110	M120
Observed events	260	3	7	3
Total expected bkg events	300 ± 40	4.8 ± 2.2	11 ± 4	4.3 ± 1.3
Fitted $t\bar{t}$ events	181 ± 25	3.2 ± 2.0	5.1 ± 3.4	0.8 ± 0.7
Fitted WW events	71 ± 17	0.9 ± 0.4	3.1 ± 0.9	2.0 ± 0.7
Fitted $WZ - ZZ$ events	12 ± 2	0.18 ± 0.13	0.9 ± 0.4	0.7 ± 0.3
Expected Z+jets	2.9 ± 1.4	0.2 ± 0.2	0.08 ± 0.13	0.05 ± 0.06
Expected $t\bar{t}V$ events	1.7 ± 0.5	0.3 ± 0.1	0.5 ± 0.2	0.35 ± 0.11
Expected Wt events	20 ± 7	-	-	-
Events with fake leptons	14 ± 8	-	0.8 ± 0.5	0.5 ± 0.4
Signal, m($\tilde{t}_1, \tilde{\chi}_1^{\pm}, \tilde{\chi}_1^0$) = (150,120,1) GeV	610 ± 110	2.6 ± 1.9	10 ± 6	5 ± 3
Signal, m($\tilde{t}_1, \tilde{\chi}_1^{\pm}, \tilde{\chi}_1^0$) = (400,250,1) GeV	21 ± 4	8.1 ± 1.5	11.1 ± 2.2	7.6 ± 1.5
Fit inputs, expected $t\bar{t}$ events	180 ± 30	3.0 ± 2.0	4.5 ± 3.5	0.7 ± 0.8
Fit inputs, expected WW events	55 ± 9	0.7 ± 0.3	2.5 ± 0.8	1.6 ± 0.7
Fit inputs, expected $WZ - ZZ$ events	13 ± 4	0.2 ± 0.4	1.0 ± 0.7	0.8 ± 0.4
95% CL limit on $\sigma_{\text{vis}}^{\text{obs}}$[fb]	2.5	0.27	0.40	0.23
95% CL limit on $\sigma_{\text{vis}}^{\text{exp}}$[fb]	3.5	0.30	0.42	0.27

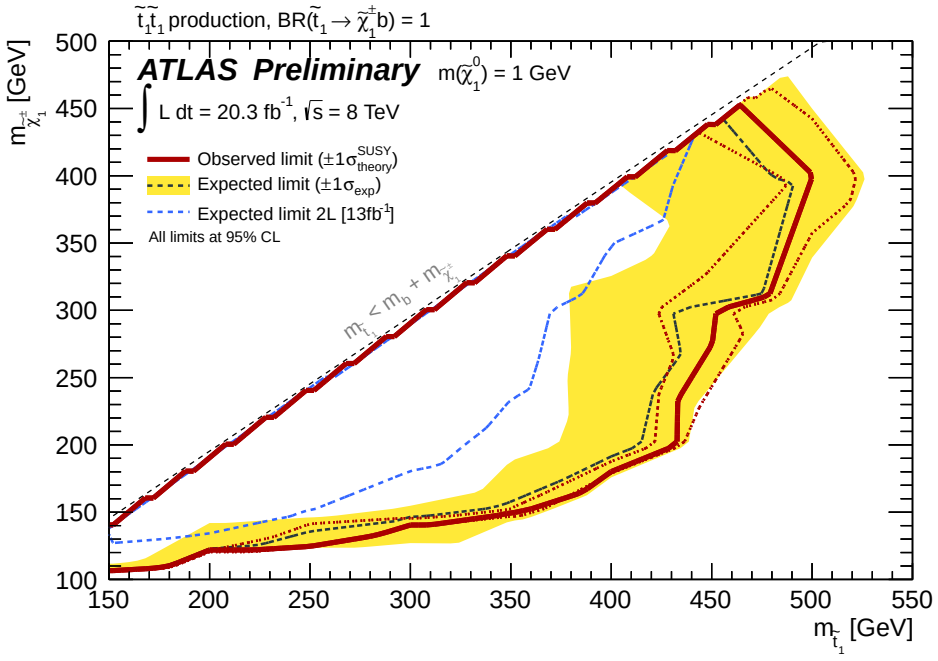

Figure 6: Exclusion limits at 95% CL from the analysis of 20.3 fb^{-1} of 8 TeV collision data on the masses of the stop and $\tilde{\chi}_1^{\pm}$, for a $\tilde{\chi}_1^0$ with a mass of 1 GeV and assuming BR($\tilde{t}_1 \to b\tilde{\chi}_1^{\pm}$) = 1. The dashed line and the shaded band are the expected limit and its $\pm 1\sigma$ uncertainty, respectively. The thick solid line is the observed limit for the central value of the signal cross section. The expected and observed limits do not include the effect of the theoretical uncertainties on the signal cross section. The dotted lines show the effect on the observed limit when varying the signal cross section by $\pm 1\sigma$ of the theoretical uncertainty. The expected limit from the previous search, based on an integrated luminosity of 13 fb^{-1}, in the two-lepton (2L) channel [24] is also shown.

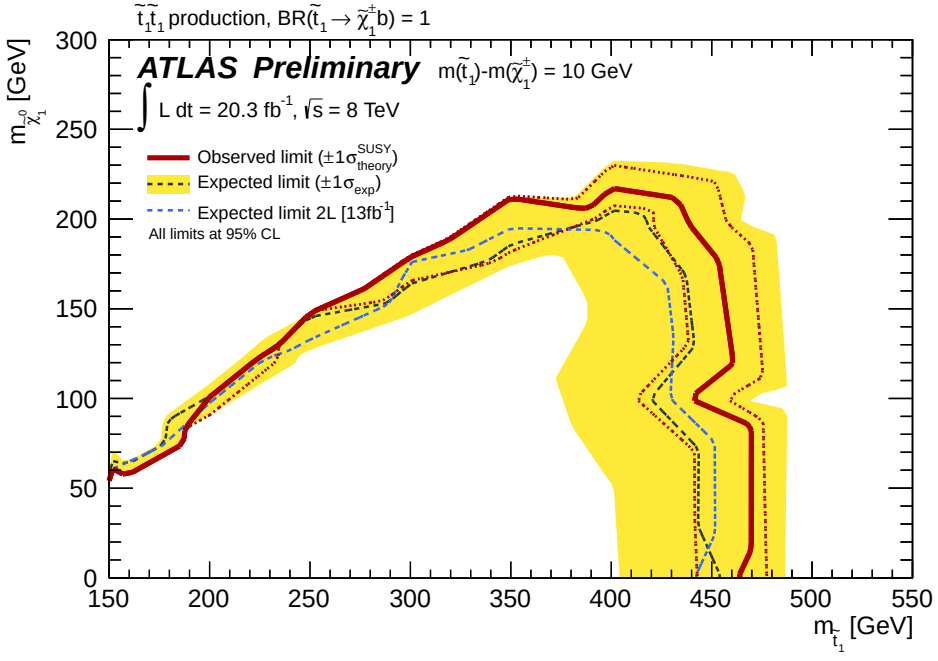

Figure 7: Exclusion limits at 95% CL from the analysis of 20.3 fb^{-1} of 8 TeV collision data on the masses of the stop and $\tilde{\chi}_1^0$, for a fixed $m(\tilde{t}_1) - m(\tilde{\chi}_1^{\pm}) = 10$ GeV and assuming BR($\tilde{t}_1 \to b\tilde{\chi}_1^{\pm}$) = 1. The dashed line and the shaded band are the expected limit and its $\pm 1\sigma$ uncertainty, respectively. The thick solid line is the observed limit for the central value of the signal cross section. The expected and observed limits do not include the effect of the theoretical uncertainties on the signal cross section. The dotted lines show the effect on the observed limit when varying the signal cross section by $\pm 1\sigma$ of the theoretical uncertainty. The expected limit from the previous preliminary search, based on an integrated luminosity of 13 fb^{-1}, in the two-lepton (2L) channel [24] is also reported.

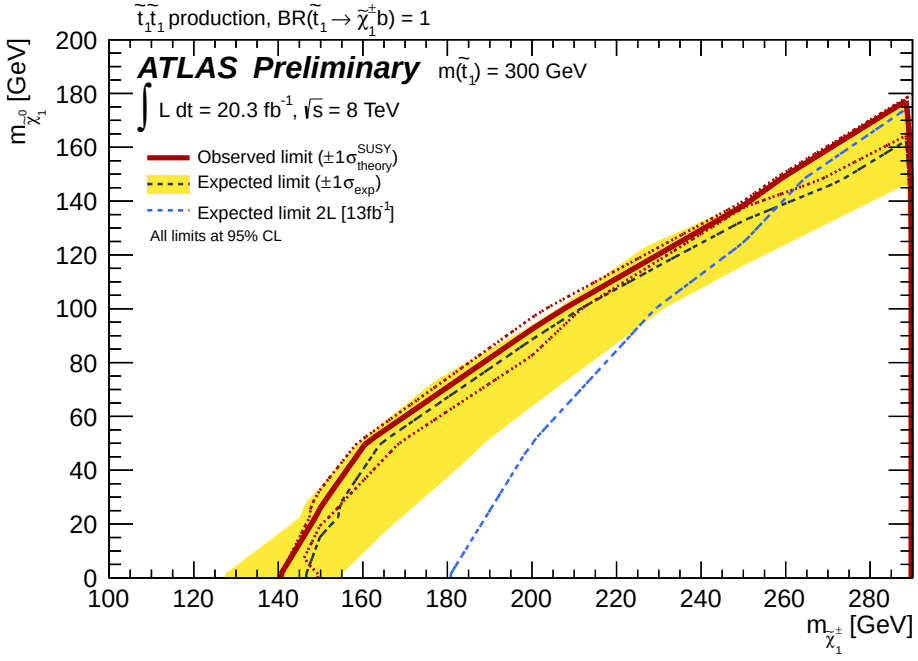

Figure 8: Exclusion limits at 95% CL from the analysis of 20.3 fb^{-1} of 8 TeV collision data on the masses of the chargino and neutralino, for a stop with a mass of 300 GeV and assuming BR($\tilde{t}_1 \rightarrow b\tilde{\chi}_1^{\pm}$) = 1. The dashed line and the shaded band are the expected limit and its $\pm 1\sigma$ uncertainty, respectively. The thick solid line is the observed limit for the central value of the signal cross section. The expected and observed limits do not include the effect of the theoretical uncertainties on the signal cross section. The dotted lines show the effect on the observed limit when varying the signal cross section by $\pm 1\sigma$ of the theoretical uncertainty. The expected limit from the previous preliminary search, based on an integrated luminosity of 13 fb^{-1}, in the two-lepton (2L) channel [24] is also reported.

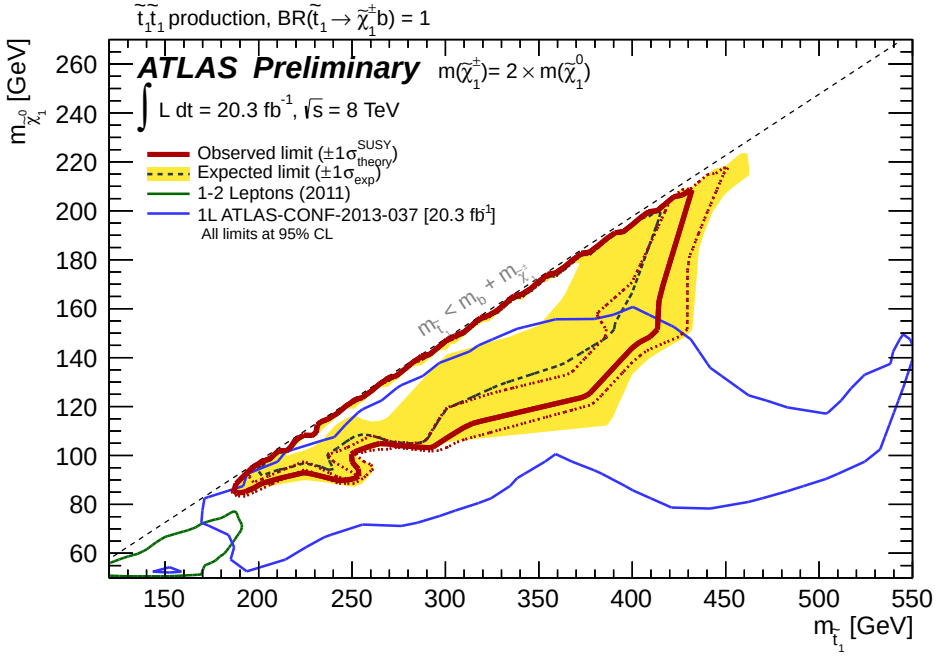

Figure 9: Exclusion limits at 95% CL from the analysis of 20.3 fb^{-1} of 8 TeV collision data on the masses of the stop and neutralino, for $m(\tilde{\chi}_1^{\pm}) = 2m(\tilde{\chi}_1^0)$ and assuming BR($\tilde{t}_1 \to b\tilde{\chi}_1^{\pm}$) = 1. The dashed line and the shaded band are the expected limit and its $\pm 1\sigma$ uncertainty, respectively. The thick solid line is the observed limit for the central value of the signal cross section. The expected and observed limits do not include the effect of the theoretical uncertainties on the signal cross section. The dotted lines show the effect on the observed limit when varying the signal cross section by $\pm 1\sigma$ of the theoretical uncertainty. The limit from the preliminary search, based on an integrated luminosity of 21 fb^{-1}, in the one-lepton (1L) channel [30] and from the published searches at $\sqrt{s} = 7$ TeV [25], based on an integrated luminosity of 4.7 fb^{-1}, are also reported.

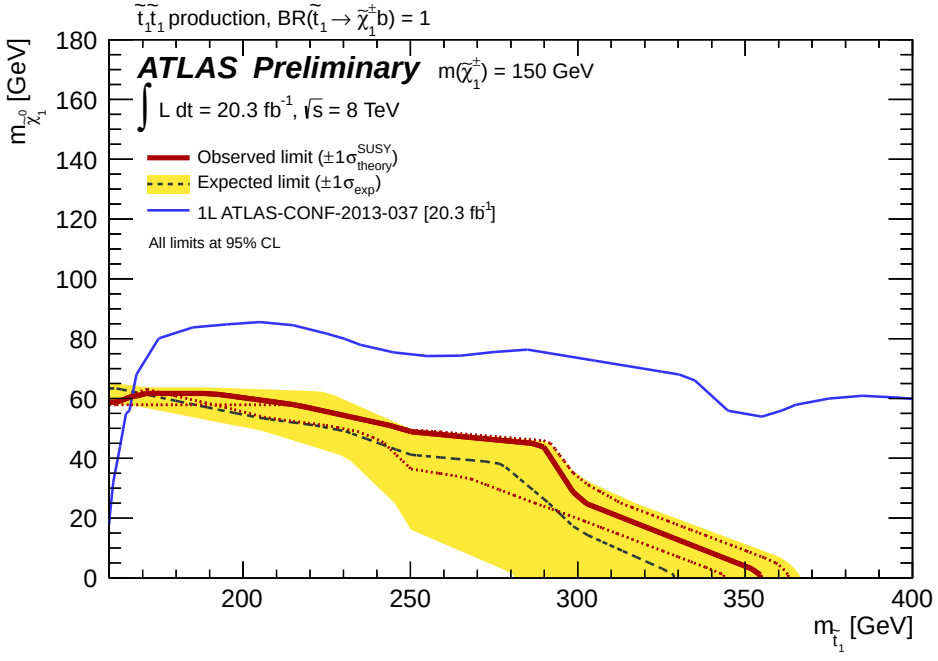

Figure 10: Exclusion limits at 95% CL from the analysis of 20.3 fb^{-1} of 8 TeV collision data on the masses of the stop and neutralino, for a chargino with a mass of 150 GeV and assuming BR($\tilde{t}_1 \to b\tilde{\chi}_1^{\pm}$) = 1. The dashed line and the shaded band are the expected limit and its $\pm 1\sigma$ uncertainty, respectively. The thick solid line is the observed limit for the central value of the signal cross section. The expected and observed limits do not include the effect of the theoretical uncertainties on the signal cross section. The dotted lines show the effect on the observed limit when varying the signal cross section by $\pm 1\sigma$ of the theoretical uncertainty. The limit from the search, based on an integrated luminosity of 21 fb^{-1}, in the one-lepton (1L) channel [30] is also reported.

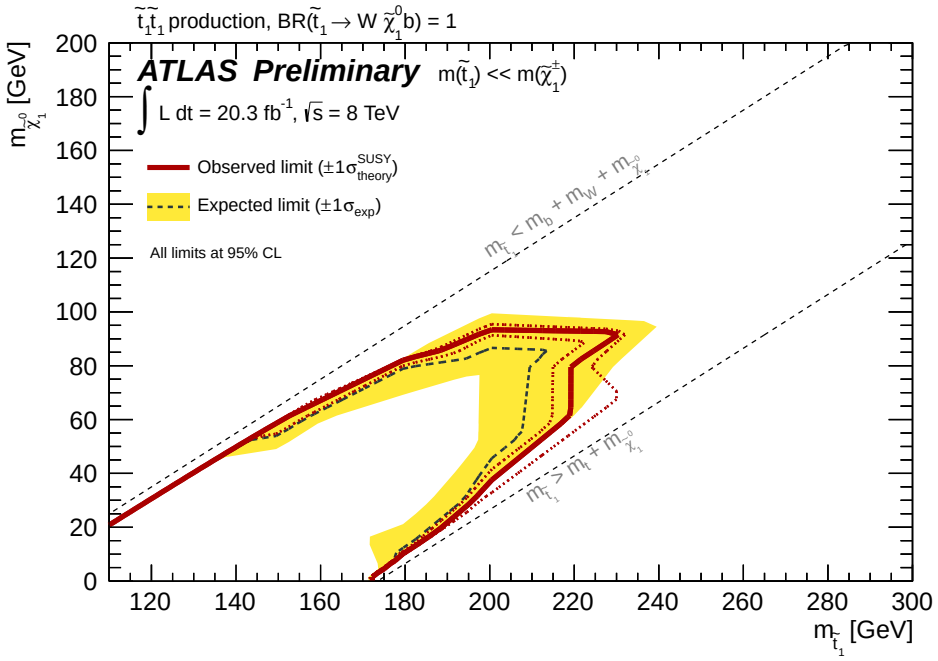

Figure 11: Exclusion limits at 95% CL from the analysis of 20.3 fb^{-1} of 8 TeV collision data on the masses of the stop and neutralino, assuming BR($\tilde{t}_1 \to Wb\tilde{\chi}_1^0$) = 1. The dashed line and the shaded band are the expected limit and its $\pm 1\sigma$ uncertainty, respectively. The thick solid line is the observed limit for the central value of the signal cross section. The expected and observed limits do not include the effect of the theoretical uncertainties on the signal cross section. The dotted lines show the effect on the observed limit when varying the signal cross section by $\pm 1\sigma$ of the theoretical uncertainty.

9 Conclusions

A search for a scalar partner of the top quark which decays into $bW\tilde{\chi}_1^0$ either directly or through an intermediate chargino state has been performed using 20.3 fb^{-1}of pp collision data at $\sqrt{s} = 8$ TeV produced by the LHC and collected by the ATLAS detector. The numbers of observed events in various signal regions have been found to be consistent with the Standard Model expectations.

Limits have been set on the mass of a supersymmetric scalar top for different assumptions on the mass hierarchy of the scalar top, the lightest chargino and the lightest neutralino. A supersymmetric top squark $\tilde{t}_1$ with a mass between 150 and 442 GeV decaying with 100% BR to a b quark and a chargino is excluded at 95% CL for a chargino approximately degenerate with the top squark and assuming a lightest neutralino with a mass of 1 GeV. Limits are also set for the first time on the direct three-body decay mode. For a value of $m(\tilde{t}_1) - m(\tilde{\chi}_1^0)$ equal to 90 GeV, 130 GeV, and 160 GeV top squark masses lower than 155 GeV, 220 GeV, and 200 GeV, respectively, are excluded.

References

[1] S. Weinberg, *Implications of Dynamical Symmetry Breaking*, Phys. Rev. **D13** (1976) 974.

[2] E. Gildener, *Gauge Symmetry Hierarchies*, Phys. Rev. **D14** (1976) 1667.

[3] S. Weinberg, *Implications of Dynamical Symmetry Breaking: An Addendum*, Phys. Rev. **D19** (1979) 1277.

[4] L. Susskind, *Dynamics of Spontaneous Symmetry Breaking in the Weinberg- Salam Theory*, Phys. Rev. **D20** (1979) 2619.

[5] L. Evans and P. Bryant, *LHC machine*, JINST **3** (2008) S08001.

[6] H. Miyazawa, *Baryon Number Changing Currents*, Prog. Theor. Phys. **36 (6)** (1966) 1266.

[7] P. Ramond, *Dual Theory for Free Fermions*, Phys. Rev. **D3** (1971) 2415.

[8] Y. Golfand and E. Likhtman, *Extension of the Algebra of Poincare Group Generators and Violation of p Invariance*, JETP Lett. **13** (1971) 323.

[9] A. Neveu and J. H. Schwarz, *Factorizable dual model of pions*, Nucl. Phys. **B31** (1971) 86.

[10] A. Neveu and J. H. Schwarz, *Quark Model of Dual Pions*, Phys. Rev. **D4** (1971) 1109.

[11] J. Gervais and B. Sakita, *Field theory interpretation of supergauges in dual models*, Nucl. Phys. **B34** (1971) 632.

[12] D. Volkov and V. Akulov, *Is the Neutrino a Goldstone Particle?*, Phys. Lett. **B46** (1973) 109.

[13] J. Wess and B. Zumino, *A Lagrangian Model Invariant Under Supergauge Transformations*, Phys. Lett. **B49** (1974) 52.

[14] J. Wess and B. Zumino, *Supergauge Transformations in Four-Dimensions*, Nucl. Phys. **B70** (1974) 39.

[15] P. Fayet, *Supersymmetry and Weak, Electromagnetic and Strong Interactions*, Phys. Lett. **B64** (1976) 159.

[16] P. Fayet, *Spontaneously Broken Supersymmetric Theories of Weak, Electromagnetic and Strong Interactions*, Phys. Lett. **B69** (1977) 489.

[17] G. R. Farrar and P. Fayet, *Phenomenology of the Production, Decay, and Detection of New Hadronic States Associated with Supersymmetry*, Phys. Lett. **B76** (1978) 575.

[18] P. Fayet, *Relations Between the Masses of the Superpartners of Leptons and Quarks, the Goldstino Couplings and the Neutral Currents*, Phys. Lett. **B84** (1979) 416.

[19] S. Dimopoulos and H. Georgi, *Softly Broken Supersymmetry and SU(5)*, Nucl. Phys. **B193** (1981) 150.

[20] C. G. Lester and D. J. Summers, *Measuring masses of semiinvisibly decaying particles pair produced at hadron colliders*, Phys. Lett. **B463** (1999) 99, arXiv:hep-ph/9906349.

[21] A. Barr, C. Lester, and P. Stephens, *m(T2) : The Truth behind the glamour*, J. Phys. **G29** (2003) 2343, arXiv:hep-ph/0304226.

[22] W. S. Cho, K. Choi, Y. G. Kim, and C. B. Park, *Measuring superparticle masses at hadron collider using the transverse mass kink*, JHEP **0802** (2008) 035, arXiv:0711.4526 [hep-ph].

[23] M. Burns, K. Kong, K. T. Matchev, and M. Park, *Using Subsystem MT2 for Complete Mass Determinations in Decay Chains with Missing Energy at Hadron Colliders*, JHEP **0903** (2009) 143, arXiv:0810.5576 [hep-ph].

[24] ATLAS Collaboration, *Search for a supersymmetric top-quark partner in final states with two leptons in $\sqrt{s}$ = 8 TeV pp collisions using 13 fb^{-1} of ATLAS data*, ATLAS-CONF-2012-167, https://cdsweb.cern.ch/record/1497733.

[25] ATLAS Collaboration, *Search for light top squark pair production in final states with leptons and b−jets with the ATLAS detector in $\sqrt{s}$ = 7 TeV proton-proton collisions*, Phys. Lett. **B720** (2013) 13, arXiv:1209.2102 [hep-ex].

[26] ATLAS Collaboration, *Search for light scalar top quark pair production in final states with two leptons with the ATLAS detector in $\sqrt{s}$ = 7 TeV proton-proton collisions*, Eur. Phys. J. **C72** (2012) 2237, arXiv:1208.4305 [hep-ex].

[27] ATLAS Collaboration, *Search for a supersymmetric partner to the top quark in final states with jets and missing transverse momentum at $\sqrt{s}$ = 7 TeV with the ATLAS detector*, Phys. Rev. Lett. **109** (2012) 211802, arXiv:1208.1447 [hep-ex].

[28] ATLAS Collaboration, *Search for direct top squark pair production in final states with one isolated lepton, jets, and missing transverse momentum in $\sqrt{s}$ = 7 TeV pp collisions using 4.7fb^{-1} of ATLAS data*, Phys. Rev. Lett. **109** (2012) 2011803, arXiv:1208.2590 [hep-ex].

[29] ATLAS Collaboration, *Search for a heavy top-quark partner in final states with two leptons with the ATLAS detector at the LHC*, JHEP 11 (2012) 094, arXiv:1209.4186 [hep-ex].

[30] ATLAS Collaboration, *Search for direct top squark pair production in final states with one isolated lepton, jets, and missing transverse momentum in $\sqrt{s}$ = 8 TeV pp collisions using 21 fb^{-1} of ATLAS data*, ATLAS-CONF-2013-037, https://cdsweb.cern.ch/record/1532431.

[31] ATLAS Collaboration, *Search for direct production of the top squark in the all-hadronic $t\bar{t} + E_{\mathrm{T}}^{\mathrm{miss}}$ final state in 21 fb^{-1} of p-p collisions at $\sqrt{s}$ = 8 TeV with the ATLAS detector.*, ATLAS-CONF-2013-024, https://cdsweb.cern.ch/record/1525880.

[32] ATLAS Collaboration, *Search for direct stop production in events with missing transverse momentum and two b-jets in $\sqrt{s}$ = 8 TeV pp collisions using 21 fb^{-1} of ATLAS data*, ATLAS-CONF-2012-171, https://cdsweb.cern.ch/record/1503233.

[33] ATLAS Collaboration, *The ATLAS Experiment at the CERN Large Hadron Collider*, JINST **3** (2008) S08003.

[34] S. Frixione, P. Nason, and C. Oleari, *Matching NLO QCD computations with Parton Shower simulations: the POWHEG method*, JHEP **0711** (2007) 070, arXiv:0709.2092 [hep-ph].

[35] T. Sjostrand, S. Mrenna, and P. Z. Skands, *PYTHIA 6.4 Physics and Manual*, JHEP **0605** (2006) 026, arXiv:hep-ph/0603175 [hep-ph].

[36] H.-L. Lai et al., *New parton distributions for collider physics*, Phys. Rev. **D82** (2010) 074024, arXiv:1007.2241 [hep-ph].

[37] G. Corcella et al., *HERWIG 6: An Event generator for hadron emission reactions with interfering gluons (including supersymmetric processes)*, JHEP **0101** (2001) 010, arXiv:hep-ph/0011363 [hep-ph].

[38] J. Butterworth, J. R. Forshaw, and M. Seymour, *Multiparton interactions in photoproduction at HERA*, Z.Phys. **C72** (1996) 637–646, arXiv:hep-ph/9601371 [hep-ph].

[39] T. Gleisberg et al., *Event generation with SHERPA 1.1*, JHEP **0902** (2009) 007, arXiv:0811.4622 [hep-ph].

[40] B. P. Kersevan and E. Richter-Was, *The Monte Carlo event generator AcerMC version 2.0 with interfaces to PYTHIA 6.2 and HERWIG 6.5*, arXiv:hep-ph/0405247 [hep-ph].

[41] ATLAS Collaboration, *Measurement of $t\bar{t}$ production with a veto on additional central jet activity in pp collisions at $\sqrt{s}$ = 7 TeV using the ATLAS detector*, Eur. Phys. J. **72** (2012) 2043, arXiv:1203.5015 [hep-ex].

[42] S. Frixione and B. R. Webber, *Matching NLO QCD computations and parton shower simulations*, JHEP **0206** (2002) 029, arXiv:hep-ph/0204244 [hep-ph].

[43] S. Frixione, E. Laenen, P. Motylinski, and B. R. Webber, *Single-top production in MC@NLO*, JHEP **03** (2006) 092, arXiv:hep-ph/0512250.

[44] J. Alwall, M. Herquet, F. Maltoni, O. Mattelaer, and T. Stelzer, *MadGraph 5 : Going Beyond*, JHEP **1106** (2011) 128, arXiv:1106.0522 [hep-ph].

[45] J. Pumplin et al., *New generation of parton distributions with uncertainties from global QCD analysis*, JHEP **0207** (2002) 012, arXiv:hep-ph/0201195 [hep-ph].

[46] S. Catani et al., *Vector boson production at hadron colliders: A fully exclusive QCD calculation at NNLO*, Phys. Rev. Lett. **103** (2009) 082001, arXiv:0903.2120 [hep-ph].

[47] A. D. Martin, W. J. Stirling, R. S. Thorne, and G. Watt, *Parton distributions for the LHC*, Eur. Phys. J. **C63** (2009) 189, arXiv:0901.0002 [hep-ph].

[48] M. Aliev et al., *HATHOR: HAdronic Top and Heavy quarks crOss section calculatoR*, Comput. Phys. Commun. **182** (2011) 1034, arXiv:1007.1327 [hep-ph].

[49] N. Kidonakis, *Two-loop soft anomalous dimensions for single top quark associated production with a W- or H-*, Phys. Rev. **D82** (2010) 054018, arXiv:1005.4451 [hep-ph].

[50] T. Binoth, M. Ciccolini, N. Kauer, and M. Krämer, *Gluon-induced W-boson pair production at the LHC*, JHEP **0612** (2006) 046, arXiv:hep-ph/0611170 [hep-ph].

[51] A. Lazopoulos, T. McElmurry, K. Melnikov, and F. Petriello, *Next-to-leading order QCD corrections to $t\bar{t}Z$ production at the LHC*, Phys. Lett. **B666** (2008) 62, arXiv:0804.2220 [hep-ph].

[52] M. Bähr et al., *Herwig++ Physics and Manual*, Eur. Phys. J. **C58** (2008) 639, arXiv:0803.0883 [hep-ph]. 143 pages, program and additional information available from http://projects.hepforge.org/herwig.

[53] W. Beenakker, M. Krämer, T. Plehn, M. Spira, and P. M. Zerwas, *Stop production at hadron colliders*, Nucl. Phys. **B515** (1998) 3, hep-ph/9710451.

[54] W. Beenakker et al., *Supersymmetric top and bottom squark production at hadron colliders*, JHEP **1008** (2010) 098, arXiv:1006.4771 [hep-ph].

[55] W. Beenakker et al., *Squark and gluino hadroproduction*, Int. J. Mod. Phys. **A26** (2011) 2637, arXiv:1105.1110 [hep-ph].

[56] M. Krämer, A. Kulesza, R. van der Leeuw, M. Mangano, S. Padhi, T. Plehn, and X. Portell, *Supersymmetry production cross sections in pp collisions at $\sqrt{s} = 7$ TeV*, arXiv:1206.2892.

[57] ATLAS Collaboration, *First tuning of HERWIG/JIMMY to ATLAS data*, ATL-PHYS-PUB-2010-014, http://cdsweb.cern.ch/record/1303025.

[58] ATLAS Collaboration, *Charged particle multiplicities in p p interactions at $\sqrt{s} = 0.9$ and 7 TeV in a diffractive limited phase-space measured with the ATLAS detector at the LHC and new PYTHIA6 tune*, ATL-CONF-2010-031, http://cdsweb.cern.ch/record/1277665.

[59] ATLAS Collaboration, *The ATLAS Simulation Infrastructure*, Eur. Phys. J. **C70** (2010) 823, arXiv:1005.4568 [physics.ins-det].

[60] GEANT4 Collaboration, S. Agostinelli et al., *GEANT4: A Simulation toolkit*, Nucl. Instrum. Meth. **A506** (2003) 250.

[61] M. Cacciari and G. P. Salam, *Dispelling the N^3 myth for the k_t jet-finder*, Phys. Lett. **B641** (2006) 57, arXiv:hep-ph/0512210 [hep-ph].

[62] M. Cacciari, G. P. Salam, and G. Soyez, *The Anti-k(t) jet clustering algorithm*, JHEP **0804** (2008) 063, arXiv:0802.1189 [hep-ph].

[63] T. Barillari et al., *Local cluster calibration*, ATLAS-LARG-PUB-2009-001, https://cdsweb.cern.ch/record/1453787.

[64] ATLAS Collaboration, *Jet energy measurement with the ATLAS detector in proton-proton collisions at $\sqrt{s} = 7$ TeV*, Eur. Phys. J. **C73** (2013) 2304, arXiv:1112.6426 [hep-ex].

[65] ATLAS Collaboration, *Electron performance measurements with the ATLAS detector using the 2010 LHC proton-proton collision data*, Eur. Phys. J. **C72** (2012) 1909, arXiv:1110.3174 [hep-ex].

[66] ATLAS Collaboration, *Muon reconstruction efficiency in reprocessed 2010 LHC proton-proton collision data recorded with the ATLAS detector*, ATLAS-CONF-2011-063, https://cdsweb.cern.ch/record/1345743.

[67] ATLAS Collaboration, *Performance of Missing Transverse Momentum Reconstruction in Proton-Proton Collisions at 7 TeV with ATLAS*, Eur. Phys. J. **C72** (2012) 1844, arXiv:1108.5602 [hep-ex].

[68] G. Polesello and D. R. Tovey, *Supersymmetric particle mass measurement with the boost-corrected contransverse mass*, JHEP **1003** (2010) 030, arXiv:0910.0174 [hep-ph].

[69] ATLAS Collaboration, *Measurement of the top quark-pair production cross section with ATLAS in pp collisions at* $\sqrt{s}$ = 7 *TeV*, Eur. Phys. J. **C71** (2011) 1577, arXiv:1012.1792 [hep-ex].

[70] ATLAS Collaboration, *Measurement of the top quark pair production cross section in pp collisions at sqrt(s) = 7 TeV in dilepton final states with ATLAS*, Phys. Lett. **B707** (2012) 459, arXiv:1108.3699 [hep-ex].

[71] ATLAS Collaboration, *Jet energy resolution and reconstruction efficiencies from in-situ techniques with the ATLAS detector using proton-proton collisions at a center-of-mass energy* $\sqrt{s}$ *= 7 TeV*, ATL-CONF-2010-054, http://cdsweb.cern.ch/record/1281311.

[72] ATLAS Collaboration, *Improved luminosity determination in pp collisions at* $\sqrt{s}$ = 7 *TeV using the ATLAS detector at the LHC*, arXiv:1302.4393 [hep-ex].

[73] P. M. Nadolsky et al., *Implications of CTEQ global analysis for collider observation*, Phys. Rev. **D78** (2008) 013004, arXiv:0802.0007 [hep-ph].

[74] A. L. Read, *Presentation of search results: The CL(s) technique*, J.Phys. **G28** (2002) 2693.

A Additional Material

In Table 8 the number of events selected by the analysis at various stages of the selection is reported for a signal sample with $m(\tilde{t}_1) = 400$ GeV, $m(\tilde{\chi}^{\pm}) = 250$ GeV and $m(\tilde{\chi}^0_1) = 1$ GeV and with the top squark decaying as $\tilde{t}_1 \to \tilde{\chi}^{\pm} b \to W^{(*)} \tilde{\chi}^0_1 b$ with unit probability. A total of 50 000 events was generated, which satisfy the condition of having at least one true electron or muon with $p_{\mathrm{T}} > 10$ GeV. This preselection has an efficiency of 65.5%.

Table 8: Number of simulated events passing various stages of the selection for a signal sample with $m(\tilde{t}_1) = 400$ GeV, $m(\tilde{\chi}^{\pm}) = 250$ GeV and $m(\tilde{\chi}^0_1) = 1$ GeV and with the top squark decaying as $\tilde{t}_1 \rightarrow \tilde{\chi}^{\pm} b \rightarrow W^{(*)} \tilde{\chi}^0_1 b$ with unit probability. Event weights are applied to correct simulated events to data. "Isolation" include the effect of tight ID for electrons and the isolation selection for both electrons and muons. "Cleaning cuts" refer to cuts applied to remove non-collision backgrounds and detector noise.

Total events	50000
Trigger	26861.6
Cleaning cuts	26384.9
Two 10 GeV preselected leptons	3416.1
same flavour	
same flavour	1730.4
isolation	1369.5
opposite sign	1339.6
$M_{ll} > 20$ GeV	1322.3
Leading lepton p_{T}	1301.2
$\lvert M_{ll} - m_Z \rvert > 20$ GeV	963.8
$\Delta\phi_{min} > 1$	506.2
$\Delta\phi_b < 1.5$	487.3
SR M90 (same flavour)	107.5
SR M100 (same flavour)	45.8
SR M110 (same flavour)	51.8
SR M120 (same flavour)	34.3
different flavour	
different flavour	1740.6
isolation	1301.1
opposite sign	1267.6
$M_{ll} > 20$ GeV	1254.5
Leading lepton p_{T}	1233.7
$\Delta\phi_{min} > 1$	607.3
$\Delta\phi_b < 1.5$	586.1
SR M90 (different flavour)	123.7
SR M100 (different flavour)	43.3
SR M110 (different flavour)	65.8
SR M120 (different flavour)	47.4

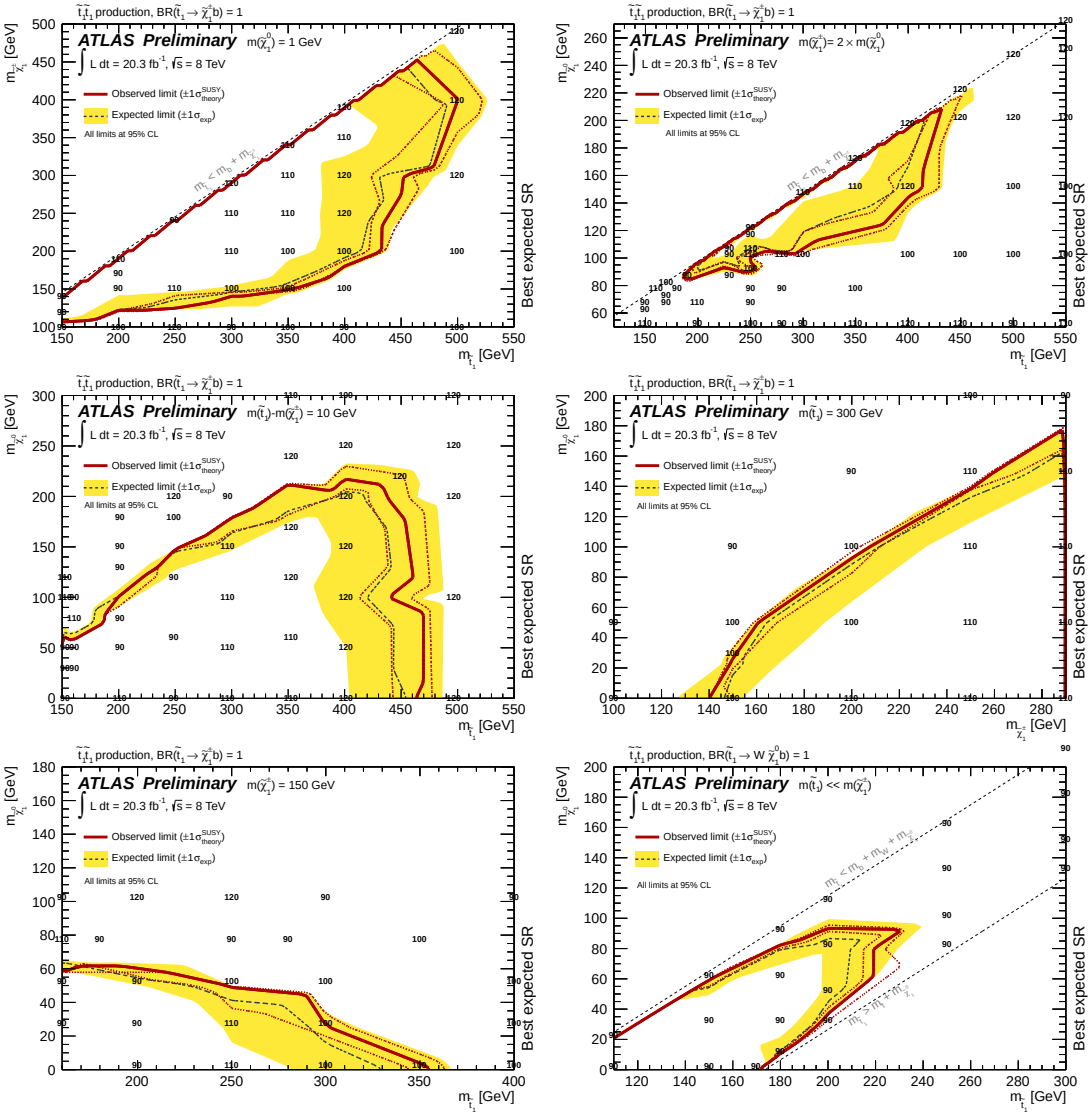

Figure 12: Illustration of the best expected SR per signal point, for the grids with BR($\tilde{t}_1 \to b\tilde{\chi}_1^{\pm}$) = 100% and a neutralino with a mass of 1 GeV (top left), $m(\tilde{\chi}_1^{\pm}) = 2m(\tilde{\chi}_1^0)$ (top right), $m(\tilde{t}_1) - m(\tilde{\chi}_1^{\pm}) = 10$ GeV (centre left), a 300 GeV top squark(centre right), a 150 GeV $\tilde{\chi}_1^{\pm}$(bottom left), and in the signal grid with BR($\tilde{t}_1 \to Wb\tilde{\chi}_1^0$) = 100% (bottom right). The M90, M100, M110 and M120 SR are indicated by their numerical values.

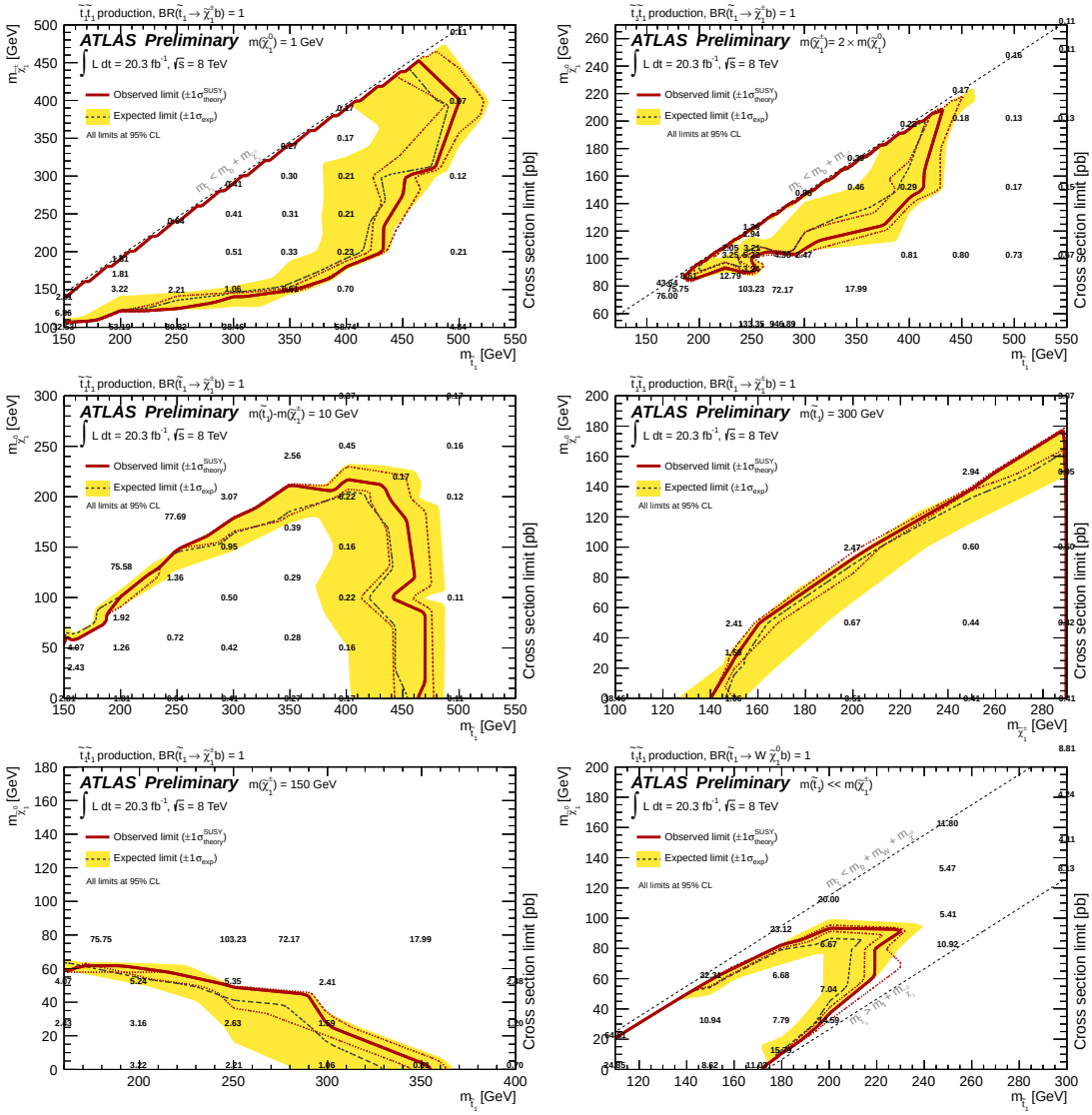

Figure 13: 95% CL limits from the analysis of 20.3 fb^{-1} of 8 TeV collision data for the grids with $\tilde{t}_1 \rightarrow b\tilde{\chi}_1^{\pm}$ and a neutralino with a mass of 1 GeV (top left), $m(\tilde{\chi}_1^{\pm}) = 2m(\tilde{\chi}_1^0)$ (top right), $m(\tilde{t}_1) - m(\tilde{\chi}_1^{\pm}) = 10$ GeV (centre left), a 300 GeV top squark(centre right), a 150 GeV $\tilde{\chi}_1^{\pm}$(bottom left), and in the signal grid with $\tilde{t}_1 \rightarrow Wb\tilde{\chi}_1^0$ (bottom right). The excluded cross section times BR for each signal point is reported. The dashed line and the shaded band are the expected limit and its $\pm 1\sigma$ uncertainty assuming the nominal cross section and 100% BR. The thick solid line is the observed limit for the central value of the signal cross section. The expected and observed limits do not include the effect of the theoretical uncertainties on the signal cross section. The dotted lines show the effect on the observed limit when varying the signal cross section by $\pm 1\sigma$ of the theoretical uncertainty.